Polarization rotation in Bi$_4$Ti$_3$O$_{12}$ by isovalent doping at the fluorite sublattice

Kevin Co,[1] Fu-Chang Sun,[1] S. Pamir Alpay,[1,2] and Sanjeev K. Nayak[1,*]

[1]*Department of Materials Science and Engineering and Institute of Materials Science,*
University of Connecticut, Storrs, Connecticut 06269, USA
[2]*Department of Physics, University of Connecticut, Storrs, Connecticut 06269, USA*

Bismuth titanate, Bi$_4$Ti$_3$O$_{12}$ (BiT), is a complex layered ferroelectric material that is composed of three perovskitelike units and one fluoritelike unit stacked alternatively along the transverse direction. The ground-state crystal structure is monoclinic with the spontaneous polarization ($\sim$50 μC/cm^2) along the plane. BiT typically grows along the c direction in thin-film form, and having the polarization vector aligned with the growth orientation can be beneficial for several potential device applications. It is well known that judicious doping of ferroelectrics is an effective method in adjusting the magnitude and the orientation of the spontaneous polarization. Here, we show using first-principles density-functional theory and a detailed phonon analysis that Bi atoms in the fluoritelike layers have significantly more impact on the magnitude and orientation of the spontaneous polarization vector as compared to the perovskitelike layer. The low-energy hard-phonon modes are characterized by fluoritelike layers experiencing transverse displacements and large changes in Born effective charges on Bi atoms. Thus, the breaking of symmetry caused by doping of Bi sites within the fluoritelike layer leads to the formation of uncancelled permanent dipole moments along the transverse direction. This provides an opportunity for doping the Bi site in the fluoritelike layer. Isovalent dopants P, As, and Sb were studied. P is found to be most effective in the reorientation of the spontaneous polarization. It leads to a threefold enhancement of the out-of-plane component of polarization and to a commensurate rotation of the spontaneous polarization vector by 36.2° towards the transverse direction.

I. INTRODUCTION

Bismuth titanate, Bi$_4$Ti$_3$O$_{12}$ (BiT), is a ferroelectric material, notable for its layered monoclinic ground-state crystal structure of the space group $B1a1$ (Pc according to the international space-group classification) [1]. The crystal structure belongs to the Aurivillius family and contains stacks of perovskitelike (PL) and fluoritelike (FL) units with a chemical formula (Bi$_2$O$_2$)(Bi$_{n-1}$Ti$_n$O$_{3n+1}$), $n \geqslant 1$ [2,3]. The crystal structure of BiT has alternating FL (Bi$_2$O$_2$)$^{2+}$ and PL (Bi$_{n-1}$Ti$_n$O$_{3n+1}$)$^{2-}$ sublayers stacked along the c axis with the number of PL layers $n = 3$. The Curie temperature of BiT is measured as $T_C = 675\,^\circ$C [2]. The ferroelectric monoclinic structure transforms to a paraelectric tetragonal crystal structure above T_C with space group $I4/mmm$. Figure 1 shows the schematic representation of the BiT crystal structure and the FL and PL layers in the paraelectric and ferroelectric states. The spontaneous polarization of BiT at 25 $^\circ$C is measured to be $\sim$50 μC/cm^2, which lies mostly parallel to the plane, and a small component of 4 μC/cm^2 appears along the transverse direction [4,5]. In comparison, the polarization value of prototypical perovskite ferroelectric compounds BaTiO$_3$ and PbTiO$_3$ are 28.4 and 66 μC/cm^2, respectively [6,7]. Due to relatively large T_C and its lead-free chemistry, BiT is an attractive ferroelectric ceramic compound that may find applications in many functional devices, including dynamic and nonvolatile memories [6,7], electrically tunable capacitors for telecommunications [8], pyroelectric sensors, piezoelectric actuators, and in high-temperature waste heat interconversion [9–14]. Layered complex oxides such as BiT are also promising materials for picoscale engineering because of a well-defined compositional and structural interface which can be controlled experimentally in a very precise manner [10].

Epitaxial BiT samples deposited by pulsed-laser deposition on a variety of substrates (such as MgO, LaAlO$_3$, SrTiO$_3$, MgAl$_2$O$_4$, and Si) typically grow preferentially along the crystallographic c axis [5,11]. This is due to the low surface energy of (001) planes leading to the nucleation of (001)-oriented platelets by an Ostwald ripening process which grow into highly textured grains to minimize grain-boundary energy [5]. Biaxial internal strains resulting from lattice mismatch in epitaxial films result in variations in the Curie transition temperature, phase transformation mode, and phase stabilities [12–19]. This misfit strain can be adjusted by varying the substrate material and by film thickness. While epitaxial strain can result in polarization rotation, previous studies on epitaxially grown stoichiometric thin films indicate that the principal component of polarization remains parallel to the growth plane [5,11,20].

Chemical alterations through judicious doping produce significant variations in the properties of ferroelectrics. Hitherto, chemical manipulation is conceived for perovskite cation sites only. Doping of the Ti site in BiT in the PL layer with La and V has led to increased chemical stability of oxygen
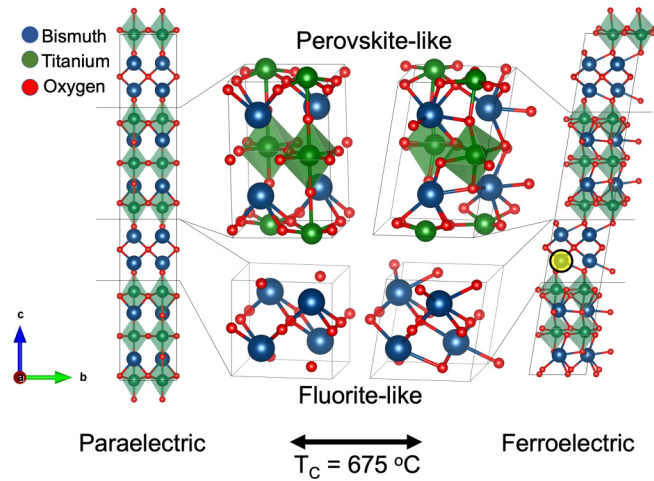
*sanjeev.nayak@uconn.edu

FIG. 1. Schematic structure of the ground-state $Ba_4Ti_3O_{12}$ projected along [010] direction (right) and the paraelectric *I4/mmm* structure (left) with zoomed projections of the local structural units (center). The monoclinic cell has the *Pc* space group. The isovalent doping Bi site (see Sec. V) is marked by a shaded circle in the monoclinic structure.

vacancies, resulting in reduced ionic and hole conductivity along the *ab* axis and highly desirable polarization-fatigue resistance [21–25]. Niobium doping at the Ti site is found to improve polarization fatigue resistance, which also led to an increase in the remanent polarization through tilting of the oxygen octahedra [7,26]. Similarly, V and W additions to the Ti site in the PL layer produce an enhancement in the remnant polarization which is believed to be related to domain phenomena [27]. Neodymium addition has been shown to result in lower remnant polarization and leakage current and tantalum doping results in lower dielectric loss [28,29]. Isovalent doping has also been explored in experiments, but is limited to PL sites [30,31]. We note that developing ferroelectric functionalities by doping with transition metals has been explored by first-principles methods but, consistent with experimental work to date, only the Ti site in the PL layer was investigated [32,33].

To date, experimental and computational studies on BiT and other ferroelectric systems clearly indicate that variations in the polarization response can be achieved by introducing chemical and structural perturbations. That being said, the possibility of reorientation of the polarization vector along the longer crystallographic transverse direction in BiT (and other Aurivillius phases) has not been explored at all. Such a study could be particularly valuable in the context of nonvolatile memory devices since it is preferable for polarization switching to develop normal to the probe direction. This would lead to a higher resolution of detecting the switching states during read and write operations [34]. It has been possible to tune the polarization rotation in artificially grown superlattice thin films, emphasizing the tunability of properties by precise control of the interface structure [35,36]. Bi site doping within PL layers with La and Nb have been carried out in a combined theoretical and experimental study and there were no significant changes in the transverse component of polarization [37]. A first-principles study on oxygen vacancies indicates that

the presence of such charged point defects do not alter the polarization direction of the material [38].

Dion-Jacobson and Ruddlesden-Popper phases are layered perovskite structures, similar to Aurivillius-type materials, characterized by perovskite units and interwoven interfacial cation layers along [001] and existing in a tetragonal phase [39–41]. In these structures, ferroelectricity is improper in its character, originating from rotations of oxygen octahedra. In contrast, the Bi_2O_2 layer of the Aurivillius phase stabilizes a monoclinic structure upon cooling, and ferroelectricity in BiT is of mixed proper-improper character [42]. Combined with the fact that the phonon density of states at low energies has maximum contributions from the Bi atoms [43], it is evident that chemical doping at the Bi sites in the Bi_2O_2 layer holds much promise in altering ferroelectric properties of BiT and BiT-like ferroelectrics. Here, we focus on the chemical manipulation of these Bi sites in the FL layer to achieve out-of-plane orientation of spontaneous polarization. Our results obtained from first-principles theory and phonon analysis indicate that Bi atoms in the FL layer have the largest contributions to the dipole moment for low-energy hard-phonon modes. This provides a unique opportunity to adjust the magnitude and the orientation of the spontaneous polarization vector by replacing the Bi ions in the FL layers with isovalent atoms such as P, As, and S. We show here that out of these P is found to be most promising in rotating the polarization vector from in-plane towards the transverse direction and in modulating the band gap, which is attractive for optoelectronic applications. These results have significant implications in designing devices with BiT and related materials.

II. COMPUTATIONAL APPROACH

First-principles calculations are performed with density-functional theory using the plane-wave pseudopotential method [44,45]. The relaxed lattice parameters for the ferroelectric monoclinic *Pc* and paraelectric tetragonal *I4/mmm* are taken from Ref. [43]. The lattice parameters for BiT in the monoclinic phase are $a = 5.49$ Å, $b = 5.53$ Å, $c = 16.88$ Å, and $\alpha = 80.61°$, $\beta = \gamma = 90°$, and for tetragonal phase, $a = b = 3.85$ Å, $c = 33.20$ Å, and $\alpha = \beta = \gamma = 90°$. It must be noted that our monoclinic structure has a axis as the unique axis, and symmetry analysis with the FINDSYM tool [46] yields the *Pc* (7) space group. The optimized structure is provided in the Supplemental Material [47]. The lattice vectors and the atomic positions of the doped models are thoroughly optimized such that there are no residual interatomic forces and the primitive cell has been expanded to contain 76 atoms. Non-spin-polarized calculations are performed with generalized gradient approximation (GGA) with Perdew-Burke-Ernzerhof parametrization [48] as the exchange-correlation functional. The core and valence electrons are treated with the projector augmented wave method [49]. The kinetic energy cutoff for the plane waves is set to 500 eV. The integrations in the Brillouin zone are performed in a discretized Monkhorst-Pack [50] k-points mesh of $5 \times 5 \times 3$ for the geometrical optimization and $8 \times 8 \times 8$ for the self-consistent field. Geometrical optimization for the models is carried out with the tolerance for total energy convergence set to 10^{-6} eV. Born effective charge (BEC) is calculated by the
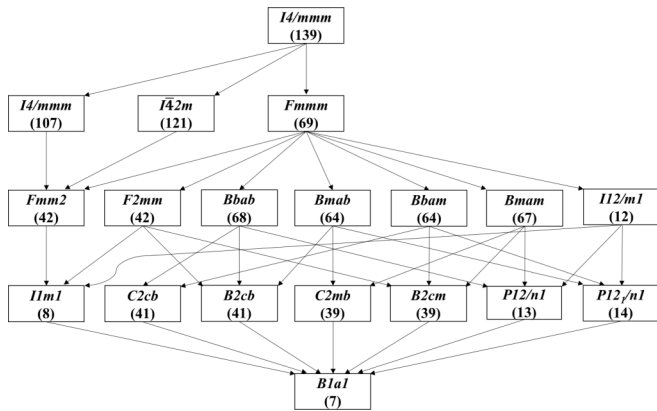
FIG. 2. Group-subgroup graph connecting the *I4/mmm* and *B1a1* space groups with all intermediate subgroups (taken from Ref. [61]).

linear response method using the density-functional perturbation theory (DFPT) [51]. The calculations are performed with the Vienna *Ab Initio* Simulation Package (VASP) [52–55]. The phonon modes are taken from a previous study [43] where PHONOPY [56] was used in the computations.

III. SPONTANEOUS POLARIZATION

According to the modern theory of polarization, the electric polarization is a differential property which is defined between the ferroelectric and the paraelectric phases of the same material [57–59]. The paraelectric reference is derived from the low-temperature phase through a continuous transformation variable which preserves the insulating character throughout the transformation. In prototype ferroelectric perovskites such as BaTiO$_3$, the transformation path is through a single symmetry-breaking transverse-optic phonon mode called the soft mode which is a characteristic of a structural phase transition [60]. BiT exhibits a more complicated phase transformation path compared to BaTiO$_3$ where multiple soft-phonon modes result in several intermediary phases through which the phase transition occurs. This is illustrated in Fig. 2 with data taken from Ref. [61]. Therefore, the paraelectric reference state must be represented by a commensurate centrosymmetric crystal structure following the principles of the modern theory of polarization. The lack of a precise transformation path for the change in crystal structure available from experiments produces only a linear mapping between the structures for density functional theory (DFT) calculations, which is often inelegant. Particular to the layered systems, there is an additional difficulty stemming from the fact that the length of one of the lattice vectors is much larger than others. This leads to smaller values of polarization quantum in the transverse directions, but the polarization components are much larger than the polarization quantum, making it difficult to track the polarization change from linear atomic displacements. Given the fact that the lattice vectors and crystal volume vary between the reference states, the polarization quantum does not remain constant throughout the intermediate images, which generates further problems in modeling.

As such, we have computed the polarization from the product of BECs and the ionic displacement vectors, taken by matching the shortest displacements between the ions of reference structures for our studies on doped BiT. The polarization component obtained from this approach is slightly larger than the reported experimental values. Since the initial and the final states are critical for the estimation of spontaneous polarization, the analysis is still useful with respect to the ferroelectric polarization, but the transformation path may not be explicitly derived from such an approach.

BECs and the atomic displacement vectors are central quantities that assist in the computation of the atomic dipole moment. Very generally, the spontaneous polarization is the integrated dipole moment over a unit volume, i.e., the dipole moment density. BEC is a tensorial quantity which is defined as the change in the polarization along a direction i induced by an atomic displacement along a direction j in the absence of external applied electric field. It is given by [57,62]

$$Z_{ij}^* = \frac{\Omega}{e} \frac{\delta P_i}{\delta d_j}, \tag{1}$$

where Ω and e are the unit cell volume and the electronic charge, respectively. The BECs computed for different atoms in the *Pc* structure of BiT are shown in Table I for PL and FL layers, where the symmetry-inequivalent atomic positions are shown in the Wyckoff notation. The BECs calculated here match with the ones reported in Ref. [63] with minor deviations that can be attributed to differences in the lattice constants. To compute the displacement vectors between ferroelectric and paraelectric BiT, it is necessary to orient the supercells such that the displacements can be matched one to one (see Fig. 1). This is achieved by applying the transformation matrices T_m and T_t to the unit cells of the monoclinic and the tetragonal lattices, respectively:

$$T_m = \begin{bmatrix} 1 & 0 & 0 \\ 0 & 1 & 0 \\ 0 & 0 & 2 \end{bmatrix}$$

$$\text{and} \quad T_t = \begin{bmatrix} \sqrt{2}\cos\left(\frac{\pi}{4}\right) & \sqrt{2}\sin\left(\frac{\pi}{4}\right) & 0 \\ -\sqrt{2}\sin\left(\frac{\pi}{4}\right) & \sqrt{2}\cos\left(\frac{\pi}{4}\right) & 0 \\ 0 & 0 & 1 \end{bmatrix}. \tag{2}$$

Atoms between the two structures are then matched first by their positions along the c axis ([001]) and the displacement vectors along the ab plane are calculated as the shortest displacement between the periodic structures. With the mapping as defined above, the y- and z components of spontaneous polarization are calculated as 52.25 and 7.88 μC/cm^2, respectively, which is in good agreement with previous DFT calculations and experimental literature [4,63]. The macroscopic value of the spontaneous polarization for the paraelectric *I4/mmm* structure is zero.

For the monoclinic structure, the off-center displacements of charges (ODCs) are central to the appearance of permanent electric dipoles and are defined by the offset distance between the cation site and neighboring oxygen cage center. In Table II, ODC averaged with the number of cations in the given sublattice and a similarly averaged cation BEC are shown for different cation positions. One clearly observes that

TABLE I. Atomic positions in the Wyckoff notation for monoclinic BiT (*Pc*) found using the FINDSYM tool [46]. The principal components of atomic BEC tensor is shown as a function of ion and sublattice [perovskitelike (PL)/fluoritelike (FL)].

Atom type	Sublattice	Wyckoff position			Born effective charge		
		x	y	z	Z^*_x	Z^*_y	Z^*_z
Bi1	PL	0.114	0.253	−0.475	5.27	4.57	4.44
Bi2	PL	0.377	0.255	−0.337	5.35	5.04	4.28
Bi3	FL	−0.334	−0.276	0.265	4.74	4.74	4.87
Bi4	FL	−0.180	0.226	0.346	4.76	4.77	4.65
Ti1	PL	0.250	0.246	0.138	7.02	5.74	5.42
Ti2	PL	0.499	0.244	0.268	6.47	5.53	5.70
Ti3	PL	−0.008	0.250	0.011	6.20	5.49	5.58
O1	PL	0.002	0.463	0.317	−4.12	−3.30	−2.07
O2	PL	0.029	0.019	−0.222	−3.72	−3.64	−2.01
O3	PL	0.366	0.171	0.248	−2.89	−2.78	−3.66
O4	PL	0.233	0.039	0.448	−4.29	−2.89	−2.34
O5	PL	0.271	−0.470	0.402	−3.99	−3.70	−2.03
O6	PL	0.366	0.171	0.248	−2.89	−2.84	−3.65
O7	PL	0.464	−0.468	0.495	−3.73	−3.68	−2.04
O8	PL	0.496	−0.053	0.086	−4.15	−3.22	−2.07
O9	FL	−0.395	0.319	0.329	−2.17	−2.05	−4.71
O10	FL	−0.257	0.009	−0.420	−2.96	−2.98	−2.76
O11	FL	−0.253	0.491	−0.082	−2.97	−2.98	−2.80
O12	FL	−0.113	0.187	−0036	−1.96	−1.85	−4.80

the y- and z components of the ODC is the largest for the Bi$_{FL}$ atoms. The numerical averages indicate that Bi ions have non-negligible contribution to polarization owing to large ODC and BEC as compared to Ti atoms. It is also worth pointing out that the number of neighboring O atoms for Bi in FL and Bi in PL layers are 8 and 6, respectively, for the monoclinic structure, while these are 12 and 8 for the *I4/mmm* structure, representing a four- and two-atom change in nearest neighbors in FL and PL. Further support for the doping of the cation site in the FL layer comes from a detailed phonon analysis which is described in the next section.

IV. PHONON ANALYSIS

Phonon analysis has been systematically used to study phase transformation and associated polarization variations in ferroelectrics [64]. Phonon modes, as used in this study, are a better approximation for accounting the ionic displacement vectors than a linear mapping between ferro- and paraelectric structures. Via this methodology, mapping the reference structures is not optimal due to the harmonic approximation; however, it provides a view of atomic contribution to dipole moments within the ferroelectric structure.

Previous studies on phonon analysis in BiT have been focused on soft phonons and structural transformation pathways for the tetragonal high-symmetry phase [61,65]. However, such approaches have not been utilized in the description of the spontaneous polarization vector. In a recent experimental study, using terahertz (THz) spectroscopy, three phonon modes in BiT were resolved having energy of 0.68, 0.86, and 0.96 THz, respectively [43]. Prior to this report, experiments reported only one phonon mode at 0.83 THz [24,66]. DFT combined with a frozen phonon method showed a normal band structure (no negative energies were observed) for the *Pc* structure, emphasizing that this structure is dynamically stable. To gain insight into the phase transformation characteristics, the ground-state monoclinic lattice is subjected here to a small perturbation described via the self-strain of the phase transformation that results in change of the monoclinic angle. The goal of such a perturbation is to approximate the onset of a thermally driven phase transition, as there are little experimental data on the intermediate states of the ferroelectric phase transition in BiT (see Fig. 2). DFPT calculations for the ground-state structure provided the energies of phonons at the Γ point which were in the following sequence: $\omega_1 = 1.108$ THz $> \omega_2 = 1.267$ THz $> \omega_3 = 1.299$ THz $< \omega_4 = 1.604$ THz.

TABLE II. The average off-center ODC between the cation atom and the nearest-neighbor oxygen atoms and the BEC for selected site-specific cations.

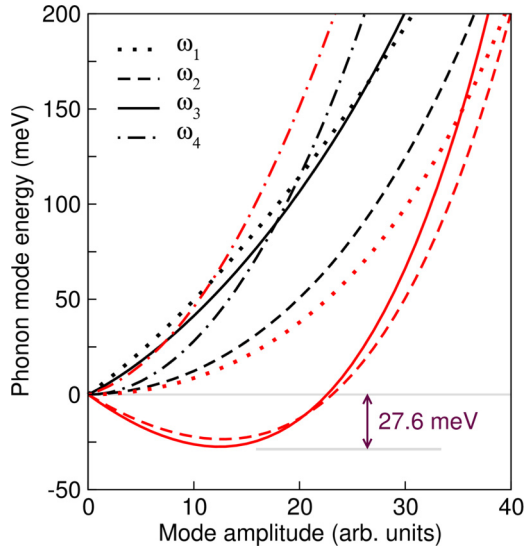| *Pc*	No. O neighbor	ODC$_x$	ODC$_y$	ODC$_z$	BEC$_x$	BEC$_y$	BEC$_z$	Nominal charge
Bi$_{Fluoritelike}$	8	0.0	0.387	−0.263	5.310	4.803	4.363	+3
Bi$_{Perovskitelike}$	6	0.0	0.202	0.032	4.750	4.758	4.762	+3
Ti$_{Perovskitelike}$	6	0.0	−0.179	0.032	6.566	5.585	5.566	+4

FIG. 3. Total energy of the supercell with respect to the ground-state energy as a function of amplitude of atomic displacements along the modes $\omega_1 - \omega_4$ for *Pc* BiT (black lines) and that obtained by shearing the lattice to increase the monoclinic angle by 0.4% (red lines). The lowering of energy as a function of mode amplitude is characteristic property for soft modes. ω_2 and ω_3 qualify as soft phonons with energy 27.6 and 25.1 meV, respectively, below ground state at nonzero amplitude. Data displayed here have been reproduced from Ref. [43].
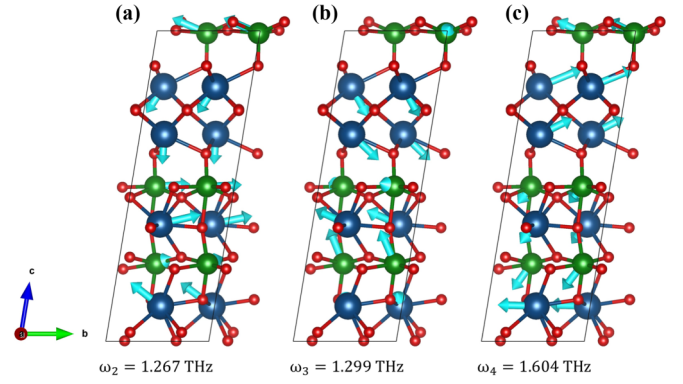

FIG. 4. Cationic phonon displacements for three low-energy phonon modes: ω_2 (a), ω_3 (b), ω_4 (c). The phonons were calculated for the monoclinic lattice under 0.04% self-strain, the tensor which is an eigenstrain due to the phase transition that converts the monoclinic phase to tetragonal phase. ω_1 is not pictured as it is characterized by transverse displacement of fluoritelike and perovskitelike layers along the nonpolar *a* axis and negligible displacement along the polar axes.

The energies of the four phonon modes as a function of their amplitude are positive and proportional to amplitude. For an angular variation of 0.04%, two of the modes, ω_2 and ω_3, lower the total energy with an increase in the phonon amplitude, see Fig. 3. The minimum energy obtained is 27.6 and 25.1 meV below the reference ground-state energy for ω_2 and ω_3, respectively. This behavior reflects a characteristic of soft modes that trigger the structural phase transition [60]. The two soft modes involve transverse displacement of FL blocks out of phase with the PL block (consistent with the rigid-layer mode defined by Machado *et al.* in Ref. [65]) for the tetragonal structures and also have components of rotation within the perovskite octahedra. There is clearly a complex interdependency of atomic displacements, volume change, and oxygen octahedra rotations that collectively carry out the phase transformation. Further, there are several intermediate phases with varying crystal symmetry as depicted in Fig. 2. As such, it is not possible to project that the soft modes derived from the monoclinic ground state are the only phase-transforming pathways for the ferroelectric transition. The soft modes could be interpreted as the restoring path to the ground state when the monoclinic structure is perturbed by the self-strain. The atomic displacements for the modes ω_2, ω_3, and ω_4 are shown by arrows in Fig. 4. The ω_1 hard mode is characterized by transverse displacement of FL and PL layers along the nonpolar *a* axis and negligible displacement along the polar axes, whereas the hard, ω_4, exhibits transverse displacements between layers along the *c* axis.

Difference in the BEC of atoms (dZ_i^*) obtained for the four phonon-displaced structures and the *Pc* reference structure as well as the atomic displacement of the phonon modes ($d\eta_i$) are then used to compute the layer-resolved dipole moment (LRDM) given by the expression

$$\text{LRDM} = \sum d\eta_i dZ_i^*. \qquad (3)$$

The *x*-, *y*-, and *z* components of LRDM are listed in Table III. The LRDM provides an insightful view of uncancelled ionic dipoles. It is observed that the FL layer has a significant influence on LRDM for the hard modes ω_1 and ω_4, implying

TABLE III. Components and absolute value of site and LRDM (%) [see Eq. (3)] for the four lowest optical phonon modes. The energy eigenvalues are in the order $\omega_1 < \omega_2 < \omega_3 < \omega_4$.

| Phonon frequency	Site type	(LRDM)$_x$	(LRDM)$_y$	(LRDM)$_z$	abs (LRDM)
	Bi	1.133	−0.060	0.807	1.395
	Ti	0.012	−0.495	0.140	0.515
ω_1	O	−0.145	1.555	0.052	0.218
	Fluorite layer	1.094	1.378	0.833	1.947
	Perovskite layer	−0.108	0.116	0.027	0.161
	Bi	−0.426	−2.635	−1.042	2.865
	Ti	−1.376	−6.071	−0.722	6.267
ω_2	O	2.802	9.706	0.230	10.105
	Fluorite layer	−0.255	0.869	−0.596	1.084
	Perovskite layer	2.631	6.176	2.326	7.105
	Bi	−0.293	1.755	−0.133	1.784
	Ti	−0.961	−4.151	−0.381	4.278
ω_3	O	2.254	3.396	1.514	4.348
	Fluorite layer	0.148	−0.355	−0.238	0.452
	Perovskite layer	2.107	5.519	1.619	6.125
	Bi	−0.343	−1.922	3.583	27.316
	Ti	−1.737	0.448	−11.274	4.080
ω_4	O	0.959	2.475	8.690	11.416
	Fluorite layer	0.320	2.202	−15.0	15.164
	Perovskite layer	2.417	−1.641	27.316	27.472
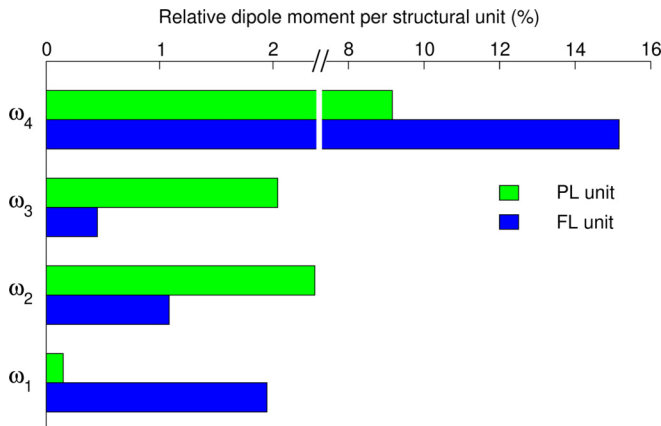
FIG. 5. The dipolar contributions per layer of fluoritelike and perovskitelike layers. The fluoritelike layer contribution is larger for the hard modes ω_1 and ω_4, while the perovskitelike layer contribution is larger for the soft modes ω_2 and ω_3 (see text for detailed discussions).

greater contribution from Bi atoms, which surpass the impact of Ti atoms. This observation further reinforces the idea of targeting the FL layer Bi atoms for controlling the properties in BiT and, more generally, the transition metal in the FL in Aurivillius-type ceramics.

The changes in the atomic dipole contributions per structural unit (FL and PL units) are summarized in Fig. 5. Here, it is clear that the involvement of the PL layer is larger for the soft modes ω_2 and ω_3. This is expected through the phenomenological understanding of polarization variations occurring via soft-mode-driven displacements [60]. For the hard mode ω_4, which is characterized by transverse displacement of the FL and PL layers along the c direction, the LRDM of the FL layer is greater than that of the PL and is mostly due to the presence of Bi atoms. These results clearly indicate that doping the Bi site in FL layers should produce significant alterations in the magnitude of the dipole moments. Furthermore, Bi atoms constitute the majority of the phonon density of states at low energies (see inset of Fig. 4 in Ref. [43]). Considering that there are transverse displacements associated with the hard mode ω_4 [see Figs. 4(c) and 5)], one would also expect a reorientation of the polarization vector towards the transverse direction.

V. ISOVALENT DOPING

It is emphasized thus far that the Bi atoms in the FL layer effectively carry the control of polarization response of BiT through transverse displacements along the z direction. An effective way of inducing specific changes in crystal structure, phonon modes, and the polarization is by doping. We studied the polarization changes due to doping for the Bi atoms in the FL layer by isovalent elements to Bi. Group 15 elements P, As, and Sb in the Periodic Table are chosen as dopants, assuming these preserve the host crystal structure. The doping concentration corresponds to 6.25%, which can be practically achievable by nonequilibrium synthesis methods such as pulsed-laser deposition. Nitrogen is excluded in the study due to the large size difference between N and Bi

TABLE IV. Computed values of components of spontaneous polarization and its norm ($\mu C/cm^2$), polar angle (degrees), and band gap (eV) for pure and doped BiT.

	P_x	P_y	P_z	P	Polar angle	Band gap
Unstrained	0.0	52.255	7.879	52.847	81.425	2.173
P doped	2.642	47.955	35.031	59.445	53.852	1.386
As doped	2.923	45.806	23.523	51.577	62.817	1.793
Sb doped	5.795	39.738	21.014	45.325	62.129	2.217

atoms. Coupled with the fact that N has a relatively high electronegativity, adding N cannot be expected to preserve the local symmetry, hence the FL structure, and the FL-PL layer arrangement necessary for the formation of a Aurivillius phase.

In these studies, the supercell geometry is optimized with respect to atomic positions to minimize residual internal forces. The optimized supercells are shown in the Supplemental Material, where it can be noted that the symmetry of the doped structures reduced to the $P1$ space group. The polarization components, absolute value of the polarization, the angle of polarization with respect to the z axis, and the band gap for different doping conditions are given in Table IV. The partial electronic density of states (PDOS) and the total electronic density of states (TDOS) are shown for P-, As-, and Sb-doped systems in Figs. 6(a)–6(c) and 6(d)–6(f), respectively. The dopant atoms hybridize across the energy range of valence band of BiT. Unlike Sb, the low-lying states of P and As near the conduction band result in an effective change in the band gap, which changes systematically as one goes down the group for the choice of dopants. The wide-band-gap characteristics are preserved in the doped BiT. P and As doping results in a 36.2% and 17.5% reduction in the band gap, respectively, while Sb doping results in a 2.0% increase as obtained from GGA calculations. It must be noted that GGA underestimates the band gap in semiconductors; however, the trends across the band gap with doping is expected to hold true to the real system. The polarization change appears on the order of few percent as compared to pure BiT, with P resulting in a slightly larger value of polarization than undoped BiT. The polarization vector is observed to have a relatively larger z component than that of the pure BiT. The polarization is rotated towards the transverse direction for all three dopants, but the highest rotation is observed for the P-doped cases, which corresponds to a threefold enhancement of the transverse component of polarization, and a commensurate rotation of the spontaneous polarization vector to 36.2° out of plane. As and Sb doping result in spontaneous polarization vectors of 27.2° and 27.9°, respectively, and lower magnitudes of polarization, as compared to P doping.

VI. STABILITY OF DOPED BiT

In order to compare the doping stability of isovalent ions on the Bi site in the FL layer, we have carried out computations related to the energetics of point defects through the calculation of formation energies ($E_{\text{Formation}}$), which is given
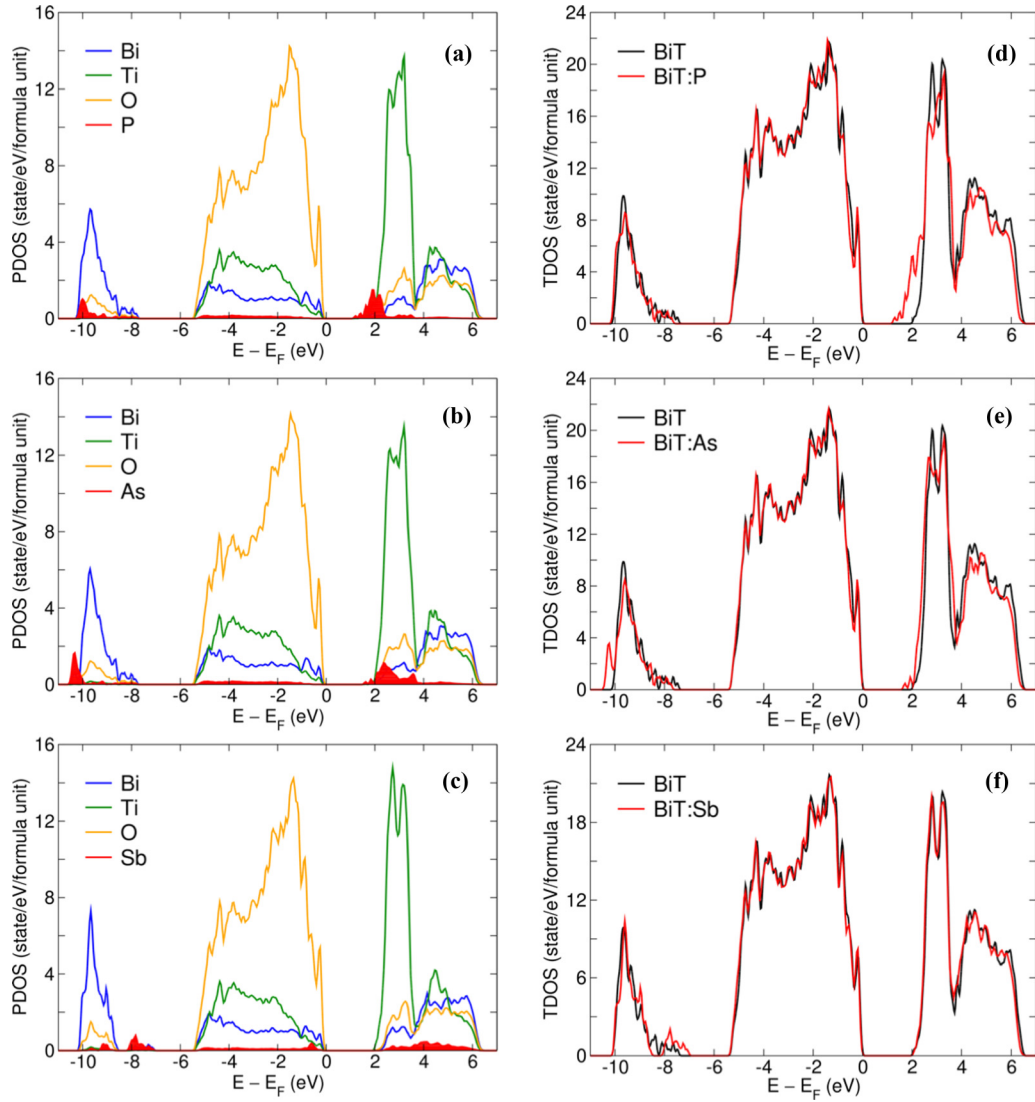
FIG. 6. Atom-resolved density of states for (a) P-, (b) As-, and (c) Sb-doped BiT and TDOS for the doped system compared to pure BiT (d)–(f). The dopant atoms show stronger hybridization. The dopant atom in the conduction band reduced the effective band gap for P and As.

by [67–70]

$$E_{\text{Formation}} = E(D) - E(\text{BiT}) + \sum_i p_i n_i \mu_i. \quad (4)$$

Here, $E(D)$ and $E(\text{BiT})$ are the total energies of the doped supercell and the pure BiT supercell of similar size, respectively. The equation is balanced via the last term by using the chemical potentials (μ_i) of the elemental species (i), their number n_i, and the factor p_i, where $p_i = -1$ for atoms added to the host supercell and $p_i = +1$ for atoms removed from the host supercell in order to construct the defect supercell. The formation energy analysis is performed for neutral charge states of the impurities. The supercell for the energy calculation contains a total of 76 atoms, which correspond to four functional units of Bi$_4$Ti$_3$O$_{12}$. The formation energies of P-, As-, and Sb-doped BiT are shown as a function of chemical potential of Bi (μ_{Bi}) in Fig. 7. The chemical potential may be thought of as to correspond to the experimental synthesis/growth/deposition conditions. Hence the formation energies as a function of chemical potentials

provide clues related to thermodynamic conditions that could sustain a doping. Since doping at the Bi site is the point of investigation, the formation energies are linearly interpolated for the allowed values of μ_{Bi}. The bounding values for μ_{Bi} are derived from the low-energy crystal form of pure Bi (Bi-rich, $\mu_{\text{Bi}} = -3.898 \, \text{eV}$) and Bi$_2O_3$ (Bi-poor, $\mu_{\text{Bi}} = -6.987 \, \text{eV}$), where total energy of O$_2$ molecule is used to match the oxygen chemical potential. The optimized crystal structures of Bi compounds used to derive the chemical potentials are supplied in the Supplemental Material [47]. The results displayed in Fig. 7 support that it is possible to dope the Bi site at the FL layer with P, As, and Sb, for a wide range of Bi chemical potentials. While the formation energies of BiT:As and BiT:Sb fall off with lowering μ_{Bi}, the formation energy of BiT:P displays a relatively sharper decrease, signifying that at Bi-poor conditions P doping is more favorable than As and Sb doping. This could be explained through the chemistry of P, where the affiliation to oxygen at nearest-neighboring oxygen creates a chemical condition towards the stable bulk oxides.
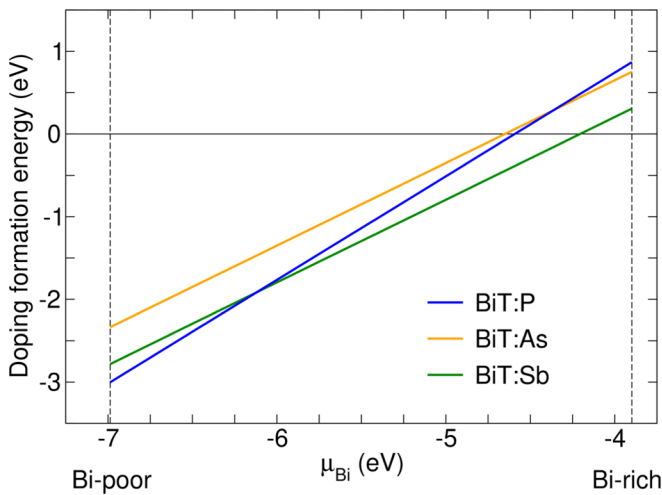
FIG. 7. Formation energy [Eq. (4)] of doping P, As, and Sb at the Bi site in fluoritelike sublattice as a function of chemical potential of Bi. The results show that the doping is favorable in Bi-poor conditions, where P is more likely to be doped as compared to As and Sb.

VII. SUMMARY

Orientation control of the spontaneous polarization vector may provide greater functionality in ferroelectric films. Stabilization of orientational variants and new rotational phases in several ferroelectric systems including $BaTiO_3$ and $PbTiO_3$ has been investigated theoretically and experimentally for over two decades [12,71]. The same concepts can be utilized in BiT and other Aurivillius systems. In particular, BiT is a promising ferroelectric due to a large polarization and high Curie temperature but is limited in applications in thin film form due to its in-plane spontaneous polarization. In this paper, we have shown, using first-principles methods and phonon studies, that it is the Bi ion in the FL-like layer in the BiT crystal structure that contributes to transverse displacements for low-energy hard-phonon modes and large contributions to the phonon density of states. As such, we explored isovalent doping on the Bi FL-like site as a means of inducing uncancelled dipole moments transverse to the primary axis of polarization. Based on density-functional theory, we have shown that P doping is a promising candidate for orientation control of the spontaneous polarization vector, resulting in a threefold enhancement of the transverse component of polarization and a commensurate rotation of the spontaneous polarization vector to 36.2° out of plane, while still maintaining the magnitude of polarization. Furthermore, the defect physics shows that P doping is possible in Bi-poor conditions and is more favorable than As and Sb. As the $(Bi_2O_2)^{2+}$ layer is a key characteristic of all Aurivillius compounds, FL cation site doping can be an effective method of polarization orientation control in other such materials systems with similar crystal structures.

[1] A. Shrinagar, A. Garg, R. Prasad, and S. Auluck, Acta Crystallogr. A **64**, 368 (2008).

[2] B. Aurivillius and P. H. Fang, Phys. Rev. **126**, 893 (1962).

[3] A. Peláiz-Barranco and Y. González-Abreu, J. Adv. Dielectr. **3**, 1330003 (2013).

[4] S. E. Cummins, J. Appl. Phys. **39**, 2268 (1968).

[5] R. Ramesh, K. Luther, B. Wilkens, D. L. Hart, E. Wang, J. M. Tarascon, A. Inam, X. D. Wu, and T. Venkatesan, Appl. Phys. Lett. **57**, 1505 (1990).

[6] H. H. Wieder, Phys. Rev. **99**, 1161 (1955).

[7] V. G. Bhide, M. S. Hegde, and K. G. Deshmukh, J. Am. Ceram. Soc. **51**, 565 (1968).

[8] G. Subramanyam, M. W. Cole, N. X. Sun, T. S. Kalkur, N. M. Sbrockey, G. S. Tompa, X. Guo, C. Chen, S. P. Alpay, G. A. Rossetti, K. Dayal, L. Q. Chen, and D. G. Schlom, J. Appl. Phys. **114**, 191301 (2013).

[9] J. F. Scott and C. A. Paz de Araujo, Science **246**, 1400 (1989).

[10] S. Ismail-Beigi, F. J. Walker, A. S. Disa, K. M. Rabe, and C. H. Ahn, Nat. Rev. Mater. **2**, 17060 (2017).

[11] H. Buhay, S. Sinharoy, W. H. Kasner, M. H. Francombe, D. R. Lampe, and E. Stepke, Appl. Phys. Lett. **58**, 1470 (1991).

[12] D. G. Schlom, L.-Q. Chen, C.-B. Eom, K. M. Rabe, S. K. Streiffer, and J.-M. Triscone, Annu. Rev. Mater. Res. **37**, 589 (2007).

[13] N. A. Pertsev, A. G. Zembilgotov, and A. K. Tagantsev, Phys. Rev. Lett. **80**, 1988 (1998).

[14] S. P. Alpay, J. Mantese, S. Trolier-Mckinstry, Q. Zhang, and R. W. Whatmore, MRS Bull. **39**, 1099 (2014).

[15] I. B. Misirlioglu, S. P. Alpay, F. He, and B. O. Wells, J. Appl. Phys. **99**, 104103 (2006).

[16] Q. Y. Qiu, R. Mahjoub, S. P. Alpay, and V. Nagarajan, Acta Mater. **58**, 823 (2010).

[17] R. K. Vasudevan, H. Khassaf, Y. Cao, S. Zhang, A. Tselev, B. Carmichael, M. B. Okatan, S. Jesse, L. Q. Chen, S. P. Alpay, S. V Kalinin, and N. Bassiri-Gharb, Adv. Funct. Mater. **26**, 478 (2016).

[18] A. Sharma, Z.-G. Ban, S. P. Alpay, and J. V. Mantese, Appl. Phys. Lett. **85**, 985 (2004).

[19] L. W. Martin and A. M. Rappe, Nat. Rev. Mater. **2**, 16087 (2016).

[20] S. H. Shah and P. D. Bristowe, J. Phys. Condens. Matter **22**, 385902 (2010).

[21] Y. Y. Yao, C. H. Song, P. Bao, D. Su, X. M. Lu, J. S. Zhu, and Y. N. Wang, J. Appl. Phys. **95**, 3126 (2004).

[22] M. Takahashi, Y. Noguchi, and M. Miyayama, Jpn. J. Appl. Phys. **42**, 6222 (2003).

[23] J. C. Bae, S. S. Kim, E. K. Choi, T. K. Song, W. J. Kim, and Y. I. Lee, Thin Solid Films **472**, 90 (2005).

[24] B. H. Park, B. S. Kang, S. D. Bu, T. W. Noh, J. Lee, and W. Jo, Nature (London) **401**, 682 (1999).

[25] S. H. Shah and P. D. Bristowe, J. Phys.: Condens. Matter **23**, 155902 (2011).

[26] J. K. Kim, J. Kim, T. K. Song, and S. S. Kim, Thin Solid Films **419**, 225 (2002).

[27] Y. Noguchi, I. Miwa, Y. Goshima, and M. Miyayama, Jpn. J. Appl. Phys. **39**, L1259 (2000).

[28] T. Goto, Y. Noguchi, M. Soga, and M. Miyayama, Mater. Res. Bull. **40**, 1044 (2005).

[29] S.-H. Hong, J. A. Horn, S. Trolier-McKinstry, and G. L. Messing, J. Mater. Sci. Lett. **19**, 1611 (2000).

[30] W. Li, J. Gu, C. Song, D. Su, and J. Zhu, J. Appl. Phys. **98**, 114104 (2005).

[31] O. Subohi, G. S. Kumar, M. M. Malik, and R. Kurchania, J. Phys. Chem. Solids **93**, 91 (2016).

[32] A. Y. Birenbaum and C. Ederer, Phys. Rev. B **90**, 214109 (2014).

[33] A. Y. Birenbaum, A. Scaramucci, and C. Ederer, Phys. Rev. B **95**, 104419 (2017).

[34] O. Auciello, J. F. Scott, and R. Ramesh, Phys. Today **51**, 22 (1998).

[35] J. Sinsheimer, S. J. Callori, B. Bein, Y. Benkara, J. Daley, J. Coraor, D. Su, P. W. Stephens, and M. Dawber, Phys. Rev. Lett. **109**, 167601 (2012).

[36] H. Lu, X. Liu, J. D. Burton, C. W. Bark, Y. Wang, Y. Zhang, D. J. Kim, A. Stamm, P. Lukashev, D. A. Felker, C. M. Folkman, P. Gao, M. S. Rzchowski, X. Q. Pan, C. B. Eom, E. Y. Tsymbal, and A. Gruverman, Adv. Mater. **24**, 1209 (2012).

[37] A. Roy, R. Prasad, S. Auluck, and A. Garg, Appl. Phys. Lett. **102**, 182901 (2013).

[38] T. Hashimoto and H. Moriwake, Phys. Rev. B **78**, 092106 (2008).

[39] N. A. Benedek, Inorg. Chem. **53**, 3769 (2014).

[40] B. V. Beznosikov and K. S. Aleksandrov, Crystallogr. Rep. **45**, 792 (2000).

[41] S. N. Ruddlesden and P. Popper, Acta Crystallogr. **10**, 538 (1957).

[42] N. A. Benedek, J. M. Rondinelli, H. Djani, P. Ghosez, and P. Lightfoot, Dalton Trans. **44**, 10543 (2015).

[43] D. Maurya, A. Charkhesht, S. K. Nayak, F.-C. Sun, D. George, A. Pramanick, M.-G. Kang, H.-C. Song, M. M. Alexander, D. Lou, G. A. Khodaparast, S. P. Alpay, N. Q. Vinh, and S. Priya, Phys. Rev. B **96**, 134114 (2017).

[44] R. O. Jones and O. Gunnarsson, Rev. Mod. Phys. **61**, 689 (1989).

[45] M. C. Payne, M. P. Teter, D. C. Allan, T. A. Arias, and J. D. Joannopoulos, Rev. Mod. Phys. **64**, 1045 (1992).

[46] H. T. Stokes and D. M. Hatch, J. Appl. Crystallogr. **38**, 237 (2005).

[47] See Supplemental Material at http://link.aps.org/supplemental/10.1103/PhysRevB.99.014101 for the optimized coordinates of pure and doped BiT.

[48] J. P. Perdew, K. Burke, and M. Ernzerhof, Phys. Rev. Lett. **77**, 3865 (1996).

[49] P. E. Blöchl, Phys. Rev. B **50**, 17953 (1994).

[50] H. J. Monkhorst and J. D. Pack, Phys. Rev. B **13**, 5188 (1976).

[51] S. Baroni, S. de Gironcoli, A. Dal Corso, and P. Giannozzi, Rev. Mod. Phys. **73**, 515 (2001).

[52] G. Kresse and J. Furthmüller, Comput. Mater. Sci. **6**, 15 (1996).

[53] G. Kresse and J. Furthmüller, Phys. Rev. B **54**, 11169 (1996).

[54] G. Kresse and D. Joubert, Phys. Rev. B **59**, 1758 (1999).

[55] M. Gajdoš, K. Hummer, G. Kresse, J. Furthmüller, and F. Bechstedt, Phys. Rev. B **73**, 045112 (2006).

[56] A. Togo and I. Tanaka, Scr. Mater. **108**, 1 (2015).

[57] R. D. King-Smith and D. Vanderbilt, Phys. Rev. B **47**, 1651 (1993).

[58] R. Resta, Rev. Mod. Phys. **66**, 899 (1994).

[59] R. Resta and D. Vanderbilt, in *Modern Ferroelectrics*, edited by C. Ahn and K. Rabe (Springer-Verlag, Berlin, 2007), pp. 31–68.

[60] M. E. Lines and A. M. Glass, *Principles and Applications of Ferroelectrics and Related Materials* (Oxford University Press, Oxford, 2001).

[61] J. M. Perez-Mato, P. Blaha, K. Schwarz, M. Aroyo, D. Orobengoa, I. Etxebarria, and A. García, Phys. Rev. B **77**, 184104 (2008).

[62] N. A. Spaldin, J. Solid State Chem. **195**, 2 (2012).

[63] A. Roy, R. Prasad, S. Auluck, and A. Garg, J. Phys.: Condens. Matter **22**, 165902 (2010).

[64] C.-Z. Wang, R. Yu, and H. Krakauer, Phys. Rev. B **54**, 11161 (1996).

[65] R. Machado, M. G. Stachiotti, R. L. Migoni, and A. H. Tera, Phys. Rev. B **70**, 214112 (2004).

[66] D. Nuzhnyy, S. Kamba, P. Kužel, S. Veljko, V. Bovtun, M. Savinov, J. Petzelt, H. Amorín, M. E. V. Costa, A. L. Kholkin, P. Boullay, and M. Adamczyk, Phys. Rev. B **74**, 134105 (2006).

[67] G. A. Baraff and M. Schlüter, Phys. Rev. Lett. **55**, 1327 (1985).

[68] S. B. Zhang and J. E. Northrup, Phys. Rev. Lett. **67**, 2339 (1991).

[69] S. K. Nayak, H. T. Langhammer, W. A. Adeagbo, W. Hergert, T. Müller, and R. Böttcher, Phys. Rev. B **91**, 155105 (2015).

[70] S. K. Nayak, W. A. Adeagbo, H. T. Langhammer, W. Hergert, T. Müller, and R. Böttcher, Phys. Status Solidi RRL **8**, 527 (2014).

[71] D. G. Schlom, L. Chen, C. J. Fennie, V. Gopalan, D. A. Muller, X. Pan, R. Ramesh, and R. Uecker, Mater. Res. Bull. **39**, 118 (2014).